Singular spectrum analysis for improving hyperspectral imaging based beef eating quality evaluation

Tong Qiao[a], Jinchang Ren[b], Cameron Craigie[c,d], Jaime Zabalza[e], Charlotte Maltin[c,f], and Stephen Marshall[g]

[a, b, e, g] *Centre for Excellence in Signal and Image Processing (CeSIP), Dept. of Electronic and Electrical Engineering, University of Strathclyde, 204 George Street, Glasgow, G1 1XW, UK.*
[c] *Quality Meat Scotland, Rural Centre, West Mains, Ingliston Newbridge, EH28 8NZ, UK.*
[d] *Present address: AgResearch Ruakura, 10 Bisley Road, Hamilton 3240, New Zealand.*
[f] *Present address: Biomics Ltd, Inverurie, Aberdeenshire, AB51 0LE, UK.*
[a] *E-mail: t.qiao@strath.ac.uk.*
[b] *E-mail: jinchang.ren@strath.ac.uk, tel. +44-141-5482384 for corresponding author Dr. Ren.*
[c] *E-mail: cameron.craigie@agresearch.co.nz.*
[e] *E-mail: j.zabalza@strath.ac.uk.*
[f] *E-mail: c.maltin@biomics.co.uk.*
[g] *E-mail: stephen.marshall@strath.ac.uk.*

ABSTRACT

Detecting beef eating quality in a non-destructive way has been popular in recent years. Among various non-destructive assessing methods, the feasibility of hyperspectral imaging (HSI) system was investigated in this paper. Hyperspectral images of beef samples were collected in an abattoir production line and used for predicting the beef tenderness and pH value. Support vector machine (SVM) was applied to construct the prediction equation. Before utilizing the original HSI spectral profiles directly, we propose to use singular spectrum analysis (SSA) as a pre-processing approach, where SSA has been proven to be an effective technique for time-series analysis in diverse applications. The results indicate that SSA can remove the instrumental noise of HSI system effectively and therefore improve the prediction performance.

KEYWORDS

Hyperspectral imaging, beef quality prediction, singular spectrum analysis, principal component analysis, support vector machine.

1 Introduction

As time goes, food quality control has become a significant issue to human beings. Serving as a very important source of nutrition, the quality of muscle foods including meat and fish, influences the re-purchase behavior of consumers (Weeranantanaphan et al., 2011). Considering food quality control requires non-destructive real-time monitoring on the production line, near-infrared spectroscopy (NIRS) was first established as a fast and promising tool for multi-constituent quality analysis of food materials, which has proved its feasibility especially in meat industry (Gowen et al., 2007; Weeranantanaphan et al., 2011). However, with limited spatial information, internal constituent gradients within food products could not be captured by NIRS, leading to discrepancies between predicted and measured composition (Gowen et al., 2007). Therefore, multispectral imaging (MSI) system, combining images at a small number of narrow wavebands, was developed afterwards to overcome the above mentioned drawbacks and has demonstrated its success for detection of meat quality (Dissing et al., 2013; Panagou et al., 2014). Through capturing hundreds of continuous bands at different wavelengths, hyperspectral imaging (HSI), as an updated version of MSI, has received considerable attention in recent years since it can acquire the spatial and spectral information simultaneously. The information contained in the HSI cube can be utilized in many areas, going from traditional applications in agricultural land use analysis with remote sensing (Lee et al., 2010; Prabhakar et al., 2011; Qiao et al., 2014) and military surveillance (Gill et al., 2011; Zhao et al., 2013) to newly emerging platforms for biomedical imaging (Wang et al., 2013) and non-invasive food quality control and analysis (Baiano et al., 2012; Gowen et al., 2009; Kelman et al., 2013; Naganathan et al., 2008; Sun,

2010). Due to the fact that HSI could collect more information than NIRS and MSI during the same time, there is a growing trend to investigate its ability to predict meat quality in a way that is fast, non-destructive and requires no reagent. In this paper, beef was chosen as a representative of muscle foods since it contributes most to the meat market in EU with 8,000,000 tonnes annual consumption and similar levels of production (Panagou et al., 2014).

Usually, for both NIRS and HSI, pre-processing of the spectral profile is needed, to eliminate undesired effects and noise produced during the data collection process. Common pre-processing techniques, especially for NIRS, include calculating derivatives, standard normal variate (SNV) and multiplicative scatter correction (MSC) (Rinnan et al., 2009). However, using derivatives of spectra may even enhance the noise and lead to more difficult spectral interpretation. For SNV and MSC, it is required to apply these transformations to all spectra as the corrected spectra would be more accurate if more spectra were involved, which is infeasible in the abattoir. In practice, ideally a prediction model based on HSI will be installed in the abattoir production line, and for every single piece of beef steak, the model should predict the quality assessment result in a real-time manner. Therefore, it is necessary to use a pre-processing technique that can be applied to every single spectrum itself, without considering other spectra. In this paper, we mainly demonstrate that singular spectrum analysis (SSA) can be regarded as an optimal pre-processing step in de-noising HSI beef spectra, where it will not be restricted by the number of HSI samples. With the beef eating quality references available as ground truth, the support vector machine (SVM), which is a state-of-the-art non-linear regression technique, was employed for data regression. Compared to other regression methods, SVM does not ask for a large amount of training samples to construct the calibration equation. Additionally, it is not affected by sample outliers either (Burges, 1999).

77 The remaining sections of this paper are organized as follows. In Section 2, sample
78 preparation and collection are presented. Besides, algorithms employed in the experiments
79 will be explained as well. Experimental results and conclusion are given in Section 3 and 4
80 respectively.

81 2 Materials and methods

82 2.1 HSI system

83 A push-broom HSI system (Gilden photonics) with wavelength ranging from 283 to 863 nm
84 at a spectral resolution of about 2.5 nm was used to collect beef data samples. Fig. 1 shows a
85 schematic diagram of the imaging system, which consists of a charge-coupled device (CCD)
86 camera, a spectrograph with lens that utilizes a wavelength dispersive system to acquire all
87 wavelengths of a single spatial line simultaneously, a tungsten halogen lamp, a sliding track
88 and a black tray for the beef. With the targeted object sliding through the imaging system, a
89 three dimensional HSI cube can be formed. Before the image collection starts, a spectral
90 calibration procedure has to be done at two extreme illuminating conditions, using a white
91 tile that reflects almost 100% of the radiation at all working wavelengths and also the lens
92 cap to get a dark image. These steps make sure that the sample reflectance can be
93 separated from the system response (Naganathan et al., 2008). Eq.(1) shows the calibration
94 calculation,

95 $$R = \frac{I - B}{I_W - B}, \tag{1}$$

96 where I, I_W and B stand for intensities of the raw image and white/dark reference images,
97 respectively.

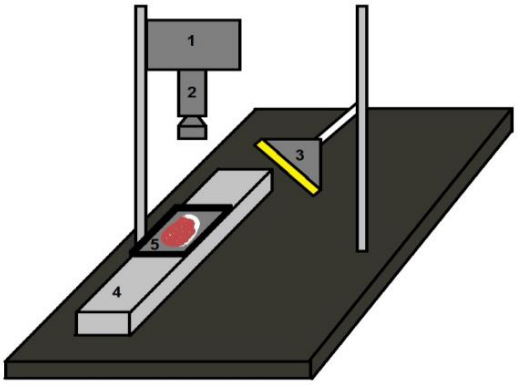

Fig. 1. Schematic diagram of a visible HSI system: components 1-5 refer to the CCD camera, spectrograph and lens, halogen lamp, sliding track and scanning tray, respectively.

2.2 Sample preparation and HSI data collection

Over 200 carcasses (*M. longissimus* muscle), which are aged for 48 hours, were randomly selected in an abattoir production line during two consecutive days, irrespective of gender, conformation, fatness, weight or maturity. For each carcass, a piece of steak with thickness of 25 mm was recovered from the 11th rib position of the strip loin.

Allowing for two minutes of blooming, hyperspectral images were collected. After imaging, each steak was divided into lateral and dorsal halves, labelled and vacuum packaged. The lateral halves were further aged for 5 days and the dorsal halves were aged for 12 days at -1 ºC before freezing. A temperature data logger was packed with each batch in order to verify the temperature during the aging process. Thus, these steaks had a total aging time of 7 days and 14 days before quality parameter measurements.

2.3 Sample quality reference measurements

Tenderness, juiciness and flavor of beef are considered as the most important attributes that influence the repurchase behavior of consumers (Shackelford et al., 2001). In our experiments, slice shear force (SSF) was measured as the tenderness reference, while the ultimate pH is found to have a strong relationship with juiciness and flavor of beef steaks. On the day before tenderness and pH tests, steaks were thawed overnight at ambient

temperature and ultimate pH values were first measured using a calibrated Hanna meat pH meter (HI 99163) without the knife blade attached. Two measurements were taken at different locations and averaged to give the final result. For offline SSF measurement, steaks were cooked on a clam-shell grill until the center temperature reached 71 ºC using a stainless steel temperature probe. Samples were sheared perpendicular to the muscle fiber axis with a Tenderscot tenderometer (Pentland Precision Engineeris, Loanhead, Midlothian), and the highest force during the shear process was picked up as the SSF. In summary, there are four beef quality attributes in total for each steak that need to be predicted, which are SSF7, SSF14, pH7 and pH14.

2.4 Singular spectrum analysis

As a relatively new technique, SSA is commonly used for time series analysis and forecasting. Based on the singular value decomposition (SVD), it is able to decompose the original time series into a few components, including the 'clean' series, oscillations and noise (Zabalza et al., 2014b). The algorithm of SSA is briefly introduced as follows.

The first step in the SSA algorithm is to transform the investigated series into the trajectory matrix. Assume we have a one dimensional series vector with length N as $\mathbf{X}=(x_1,\cdots,x_N)$. Given a window length L $(1<L<N)$, the initial series can be mapped into K lagged vectors, $\mathbf{X}_i=(x_i,\cdots,x_{i+L-1})^{\mathrm{T}}$ for $i=1,\cdots,K$, where $K=N-L+1$. Then, the trajectory matrix is formed as Eq.(2). One thing worth of noting is that the matrix $\mathbf{T}$ is a Hankel matrix with size of $L\times K$, where $\mathbf{T}$ has equal elements x_{ij} on the anti-diagonals where $i+j=\text{const}$,

$$\mathbf{T}=\begin{pmatrix}\mathbf{X}_1 & \mathbf{X}_2 & \cdots & \mathbf{X}_K\end{pmatrix}=\begin{pmatrix}x_1 & x_2 & \cdots & x_K\\ x_2 & x_3 & \cdots & x_{K+1}\\ \vdots & \vdots & \ddots & \vdots\\ x_L & x_{L+1} & \cdots & x_N\end{pmatrix}. \quad (2)$$

The next step is to perform the SVD of the trajectory matrix $\mathbf{T}$. First, the eigenvalues of $\mathbf{T}\mathbf{T}^{\mathrm{T}}$ are calculated and arranged in the decreasing order, written as $\left(\lambda_1 \geq \cdots \lambda_L \geq 0\right)$. The corresponding eigenvectors are denoted as $\left(U_1, \cdots, U_L\right)$. Then the result of SVD is shown in Eq.(3),

$$\mathbf{T} = \mathbf{T}_1 + \cdots + \mathbf{T}_d, \tag{3}$$

where d is the rank of $\mathbf{T}$, $\mathbf{T}_i = \sqrt{\lambda_i}\mathbf{U}_i\mathbf{V}_i^{\mathrm{T}}$ $\left(i = 1, \cdots, d\right)$ are called elementary matrix with rank 1, and $\mathbf{V}_i = \mathbf{T}^{\mathrm{T}}\mathbf{U}_i / \sqrt{\lambda_i}$ are often called principal components of the matrix $\mathbf{T}$. In general, the contribution of $\mathbf{T}_i$ to the trajectory matrix $\mathbf{T}$ depends on the ratio of each eigenvalue and the sum of these eigenvalues, shown in Eq.(4),

$$\eta_i = \lambda_i / \sum_{i=1}^{d} \lambda_i. \tag{4}$$

The following step of SSA is called grouping, where the set of indices $\left\{1, \cdots, d\right\}$ is divided into m disjointed subsets $I_1, \cdots, I_m$. Assume $I = \left\{i_1, \cdots, i_p\right\}$, then the trajectory matrix corresponding to the group I is defined as $\mathbf{T}_I = \mathbf{T}_{i_1} + \cdots + \mathbf{T}_{i_p}$. Similarly, the resultant trajectory matrices can be calculated for every group $I = I_1, \ldots, I_m$ and Eq.(3) is expanded as Eq.(5),

$$\mathbf{T} = \mathbf{T}_{I_1} + \cdots + \mathbf{T}_{I_m} \tag{5}$$

The last step is the diagonal averaging which first hankelizes the grouped matrices $\mathbf{T}_I$ and then transforms them into a new series with length N. Let $\mathbf{Y}_1 = (y_1, \cdots, y_N)$ be the transformed one dimensional series of $\mathbf{T}_{I_1}$, elements in $\mathbf{Y}_1$ can be represented as Eq.(6),

157
$$y_k = \begin{cases} \frac{1}{k}\sum_{j=1}^{k} y^*_{j,k-j+1}, & \text{for} \quad 1 \le k < L^* \\ \frac{1}{L^*}\sum_{j=1}^{L^*} y^*_{j,k-j+1}, & \text{for} \quad L^* \le k \le K^* \\ \frac{1}{N-k+1}\sum_{j=k-K^*+1}^{N-K^*+1} y^*_{j,k-j+1}, & \text{for} \quad K^* < k \le N, \end{cases} \tag{6}$$

158 where $L^* = \min(L,K)$, $K^* = \max(L,K)$, $y^*_{j,k-j+1} = y_{j,k-j+1}$ if $L < K$ and $y^*_{j,k-j+1} = y_{k-j+1,j}$ if $L \ge K$.

159 Hence, the initial series $\mathbf{X} = (x_1, \cdots, x_N)$ can be decomposed into m series:

160
$$\mathbf{X} = \mathbf{Y}_1 + \cdots + \mathbf{Y}_m. \tag{7}$$

161 In SSA decomposition with m reconstructed series, the first reconstructed series $(\mathbf{Y}_1)$ is
162 regarded as the most important one. Hence the rest are discarded as noise.

163 2.5 HSI data pre-processing

164 The hyperspectral image data were then imported to MATLAB 2013 (MathWorks) for further
165 processing and analysis. Fig. 2(a) shows a sample image at one wavelength after reflectance
166 calibration. In order to improve the regression performance and processing speed, a region-
167 of-interest (ROI) with size of 100×200 was selected from the lean part on each
168 hyperspectral image, illustrated in Fig. 2(b). Even though most of fat area was discarded,
169 there were still a few pixels that had different spectral features from pure lean pixels, i.e.
170 dead pixels. In this context, an iterative pixel removal process (Burger and Geladi, 2006) was
171 applied to the ROI to exclude these dead pixels. For all spectra in the ROI, the Euclidean
172 distances to the median spectrum and the standard deviation of these distances were
173 calculated. Then those pixels with distances higher than five standard deviations were
174 removed from the ROI. It is assumed that in our experiments, 100 times iterations should be
175 enough for removing dead pixels. In addition, the first 50 bands were removed due to the
176 visual spatial noise presented in the images. After these cleaning steps, it is assumed that all
177 pixels in the ROI are contributed by the lean part and finally a new median spectrum in Fig.

2(c) can be achieved, shown by the full line. One thing worth of noting is that for the new median spectrum, the reflectance at each wavelength does not necessarily come from the same location in the ROI. As a result, noise could also possibly be produced during this process. As mentioned previously, we propose to use SSA for removing various noises from HSI median spectra and the result is shown by the dotted line in Fig. 2(c).

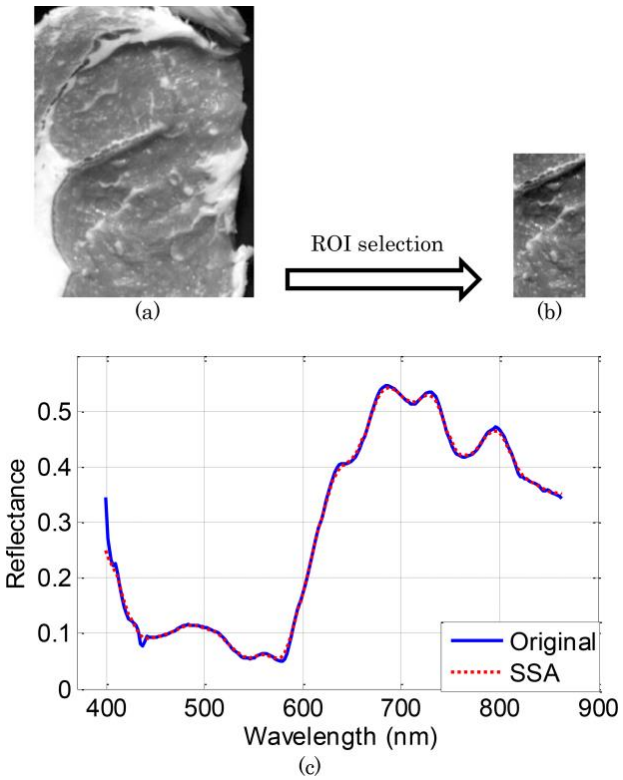

Fig. 2 HSI spectral feature extraction. (a) A band in a sample hyperspectral image, (b) ROI in the sample image, and (c) original median spectrum and SSA treated median spectrum of the ROI.

There are two important parameters that affect the performance of SSA, which are the window length L and the eigenvalue grouping. The window length determines the number of decomposed series after SSA, while the eigenvalue grouping defines how many decomposed series are used for reconstruction in order to remove noise. In our experiments, we only used the first decomposed series for spectrum reconstruction as previously discussed and the only parameter to be adjusted is the window length L. In Fig. 2(c), the

window length is set as 5. Even though a subtle difference can be noticed in the plot, it is demonstrated that SSA did improve the prediction performance as shown below.

After effective feature extraction by SSA, the reflectance spectra (R) were usually transformed into absorbance $(1/R)$ by logarithm transformation, in order to linearize the relationship between the concentration of an absorbing compound and the absorption spectrum (Rust et al., 2008).

2.6 Regression analysis model

Unlike other researchers who usually use partial least squares regression (PLSR) to build the regression model, we have employed SVM instead. The ability of SVM has been exploited in many applications associated with HSI, which is proved to be an outstanding machine learning model. However, a major problem of SVM is its curse of dimensionality. As a result, principal component analysis (PCA), as an effective feature extraction technique for hyperspectral data (Gowen et al., 2008; Ren et al., 2014; Zabalza et al., 2014a; Zabalza et al., 2014c), was introduced to reduce the dimensionality of our beef hyperspectral images.

PCA is found to be able to project the high-dimensionality data to a new space, where differentiability is higher in a subset containing first few transformed features than other subsets (Sun, 2010). Therefore, only a small amount of features would explain the high-dimensionality data and the rest of features can be discarded.

Assume $\mathbf{x}_k$ $(k=1,2,\cdots,n)$ is the reflectance spectrum of each sample with m dimensions, then the whole dataset can be represented by an $n\times m$ matrix, shown as Eq.(8):

$$\mathbf{X}=\begin{pmatrix}\mathbf{x}_1\\ \mathbf{x}_2\\ \vdots\\ \mathbf{x}_n\end{pmatrix}. \tag{8}$$

213 The first step of PCA is to find the covariance matrix of the whole data, as given in Eq.(9),

214 $$\mathbf{S}_{\mathbf{x}} = \frac{1}{n-1}\left(\mathbf{X}-\boldsymbol{\mu}\right)^{\mathrm{T}}\left(\mathbf{X}-\boldsymbol{\mu}\right), \tag{9}$$

215 where $\boldsymbol{\mu}$ is the mean spectrum of the whole dataset. The projection $\mathbf{W}_{opt}$ is chosen to
216 maximize the determinant of the total covariance matrix of the projected samples, which is

217 $$\mathbf{W}_{opt} = \arg\max\left(\mathbf{W}^{\mathrm{T}}\mathbf{S}_{\mathbf{x}}\mathbf{W}\right) = \left(\mathbf{w}_1 \quad \mathbf{w}_2 \quad \cdots \quad \mathbf{w}_L\right), \tag{10}$$

218 where $\mathbf{w}_i \ \left(i = 1,2,...,L\right)$ is the set of L dimensional eigenvectors of $\mathbf{S}_{\mathbf{x}}$ corresponding to L
219 largest eigenvalues. Thus, the dimensionality is reduced from m to L.

220 With a lower dimension L, SVM is applied to construct the prediction model. For
221 classification and regression problems, SVM maps the training dataset **x** to a high
222 dimensional feature space by using a non-linear kernel function, shown below:

223 $$K(\mathbf{x}_i, \mathbf{x}_j) = \Phi(\mathbf{x}_i)\Phi(\mathbf{x}_j), \tag{11}$$

224 where Φ is the mapping function. Then it is able to classify the data by a maximal margin
225 hyperplane. The radial basis function (RBF) kernel was selected in this paper, given in Eq.(12):

226 $$K(\mathbf{x}_i, \mathbf{x}_j) = \exp(-\gamma\left\|\mathbf{x}_i - \mathbf{x}_j\right\|^2). \tag{12}$$

227 Optimized parameters were grid-searched using four-fold cross-validation in order to avoid
228 model over-fitting.

229 3 Results and discussion

230 To test the ability of HSI for evaluating unknown beef quality, data has to be split into the
231 calibration set and the validation set, where models would be learnt from the calibration set
232 and tested on the validation set. By sorting each quality trait (SSF7, SSF14, pH7 and pH14) in

ascending order respectively and selecting every fourth sample into the validation set with the interleaving three samples being allocated to the calibration set (Williams, 2001), it ensures that the validation set is similar to the calibration set, considering the mean value, the range and the standard deviation (SD) of each analyzed quality attribute, where the statistics are shown in Table 1.

Table 1. Summary statistics of studied beef quality attributes.

Trait	Calibration set					Validation set				
	n	Min	Max	Mean	SD	n	Min	Max	Mean	SD
SSF7	159	46.97	299.54	131.46	48.18	52	69.41	285.62	130.73	45.69
SSF14	159	63.35	291.56	132.23	42.91	52	73.61	239.82	131.32	39.91
pH7	154	5.44	6.37	5.63	0.13	51	5.46	6.34	5.63	0.14
pH14	154	5.46	6.46	5.69	0.14	51	5.48	6.41	5.69	0.14

The prediction performance was evaluated quantitatively by the coefficient of determination (R^2) and the ratio of performance deviation (*RPD*). Equations for these metrics are given below:

$$R^2 = 1 - \frac{\sum_{i=1}^{n}(y_i - f_i)^2}{\sum_{i=1}^{n}(y_i - \bar{y})^2}, \tag{13}$$

$$RPD = \frac{SD}{RMSEP} = \frac{SD}{\sqrt{\frac{\sum_{i=1}^{n}(f_i - y_i)^2}{n}}}, \tag{14}$$

where y_i is the original quality trait value, f_i is the predicted trait value, $\bar{y}$ is the mean of original trait values and n is the total number of samples in the validation set. The coefficient of determination varies within 0 to 1, where 0 represents a poor correlation

between the predicted trait values and the reference trait values while 1 means a high degree of correlation.

By trial and error, the number of principal components was set as 30. In that case, dimensionality has been reduced dramatically while enough features have been preserved. Results comparing the performance of the original spectra and SSA treated spectra for the validation set are shown in Table 2. The window length *L* was tuned to achieve the best result. As highlighted in bold, except for limited improvement on SSF14, SSA could always stand out prominently, which demonstrates that it is an excellent feature extraction and de-noising pre-processing procedure for HSI spectral profiles. Just like the time series, in this paper one-dimensional (1D) SSA was applied in HSI spectral domain. Future work involves combining two-dimensional (2D) SSA on the spatial domain, which has been proved to be even more effective on remote sensing HSI based classification problems than 1D SSA (Zabalza et al., 2015).

Table 2. Performance comparison of original HSI spectra and SSA treated spectra for predicting beef eating quality attributes.

Trait	Original spectra		SSA treated spectra		
	R^2	RPD	L	R^2	RPD
SSF7	0.1938	1.1019	2	**0.3288**	**1.2082**
SSF14	0.1001	1.0264	2	0.1104	1.0249
pH7	0.4227	1.2490	3	**0.4511**	**1.2822**
pH14	0.2785	1.1234	7	**0.3419**	**1.2090**

If we adjust the number of principal components and the window length of SSA by conducting a grid search, the regression performance with the validation set can be even further improved. Chosen parameters and results for SSA treated HSI spectra are shown in Table 3.

Table 3. Best performance of SSA treated spectra for predicting beef eating quality attributes.

Trait	No. of PCs	L	R^2	RPD
SSF7	30	2	0.3288	1.2082
SSF14	20	6	0.2033	1.1048
pH7	45	2	0.5838	1.4320
pH14	45	3	0.4863	1.3615

As can be seen, for predicting ultimate pH values, both R^2 and *RPD* indicate that HSI could be a promising tool for the beef industry. However, the results for predicting SSF are not very satisfying, which might be due to the fact that SSF is not a standard quantitative metric of meat tenderness, regardless inconsistent measurements within the ground truth. Similar results have been achieved by other researchers as well. Prieto et al. (Prieto et al., 2009) have predicted SSF using NIRS, giving R^2 of 0.31 (*RPD* = 1.25) and 0.23 (*RPD* = 1.14) for SSF3 and SSF14 respectively. But, it should be noted that comparisons between studies are not reliable due to different samples used. Nevertheless, we cannot deny the potential of HSI in providing additional information that could help to improve prediction of meat quality attributes.

4 Conclusion

In conclusion, a relatively new time series analysis method named SSA is proposed to pre-process HSI spectra. By decomposing original spectra and reconstructing the spectra using the most significant components, SSA demonstrates its ability in removing noise and improving the prediction accuracy for HSI based beef eating quality evaluation. Although in this paper SSA was only applied on beef hyperspectral images, it is not limited in this field. We believe that it can be extended to other HSI based applications, including data prediction in both classification and regression problems.

Acknowledgement

The current research is funded by Quality Meat Scotland (QMS) and University of Strathclyde.

Authors would like to thank editors and anonymous reviewers for helping improving the quality of this paper.

References

Baiano, A., Terracone, C., Peri, G., Romaniello, R., 2012. Application of hyperspectral imaging for prediction of physico-chemical and sensory characteristics of table grapes. Comput. Electron. Agric. 87, 142-151.

Burger, J., Geladi, P., 2006. Hyperspectral NIR image regression part II: Dataset preprocessing diagnostics. J. Chemometr. 20 (3-4), 106-119.

Burges, C., 1999. Geometry and invariance in kernel based methods. MIT Press, Cambridge, MA.

Dissing, B., Papadopoulou, O., Tassou, C., Ersboll, B., Carstensen, J., Panagou, E., Nychas, G., 2013. Using multispectral imaging for spoilage detection of pork meat. Food Bioprocess Tech. 6 (9), 2268-2279.

Gill, K., Ren, J., Marshall, S., Karthick, S., Gilchrist, J., 2011. Quality-assured fingerprint image enhancement and extraction using hyperspectral imaging. In: Proceedings of the 4th International Conference on Imaging for Crime Detection and Prevention 2011 (ICDP 2011), London.

Gowen, A., O'Donnell, C., Cullen, P., Downey, G., Frias, J., 2007. Hyperspectral imaging – an emerging process analytical tool for food quality and safety control. Trends Food Sci. Tech. 18, 590-598.

Gowen, A., O'Donnell, C., Taghizadeh, M., Cullen, P., Frias, J., Downey, G., 2008. Hyperspectral imaging combined with principal component analysis for bruise damage detection on white mushrooms (Agaricus bisporus). J. Chemometr. 22 (3-4), 259-267.

Gowen, A., Taghizadeh, M., O'Donnell, C., 2009. Identification of mushrooms subjected to freeze damage using hyperspectral imaging. J. Food Eng. 93 (1), 7-12.

Kelman, T., Ren, J., Marshall, S., 2013. Effective classification of Chinese tea samples in hyperspctral imaging. Artif. Intell. Res. 2, 87-96.

Lee, W.S., Alchanatis, V., Yang, C., Hirafuji, M., Moshou, D., Li, C., 2010. Sensing technologies for precision specialty crop production. Comput. Electron. Agric. 74 (1), 2-33.

Naganathan, G.K., Grimes, L.M., Subbiah, J., Calkins, C.R., Samal, A., Meyer, G.E., 2008. Visible/near-infrared hyperspectral imaging for beef tenderness prediction. Comput. Electron. Agric. 64, 225-233.

Panagou, E., Papadopoulou, O., Carstensen, J., Nychas, G.J., 2014. Potential of multispectral imaging technology for rapid and non-destructive determination of the microbiological quality of beef filets during aerobic storage. Int. J. Food Microbiol. 174, 1-11.

Prabhakar, M., Prasad, Y.G., Thirupathi, M., Sreedevi, G., Dharajothi, B., Venkateswarlu, B., 2011. Use of ground based hyperspectral remote sensing for detection of stress in cotton caused by leafhopper (Hemiptera: Cicadellidae). Comput. Electron. Agric. 79 (2), 189-198.

Prieto, N., Ross, D., Navajas, E., Nute, G., Richardson, R., Hyslop, J., Simm, G., Roehe, R., 2009. On-line application of visible and near infrared reflectance spectroscopy to predict chemical–physical and sensory characteristics of beef quality. Meat Sci. 83 (1), 96-103

Qiao, T., Ren, J., Sun, M., Zheng, J., Marshall, S., 2014. Effective compression of hyperspectral imagery using an improved 3D DCT approach for land-cover analysis in re-sensing applications. Int. J. Remote Sens. 35 (20), 7316-7337.

Ren, J., Zabalza, J., Marshall, S., Zheng, J., 2014. Effective feature extraction and data reduction in remote sensing using hyperspectral imaging. IEEE Signal Process. Mag. 31 (4), 149-154.

Rinnan, A., van den Berg, F., Engelsen, S., 2009. Review of the most common pre-processing techniques for near-infrared spectra. TRAC-Trend. Anal. Chem. 28 (10), 1201-1222.

Rust, S., Price, D., Subbiah, J., Kranzler, G., Hilton, G., Vanoverbeke, D., Morgan, J., 2008. Predicting beef tenderness using near-infrared spectroscopy. J. Anim. Sci. 86 (1), 211-219

Shackelford, S., Wheeler, T., Meade, M., Reagan, J., Byrnes, B., Koohmaraie, M., 2001. Consumer impressions of Tender Select beef. J. Anim. Sci. 79 (10), 2605-2614.

Sun, D.W., 2010. Hyperspectral imaging for food quality analysis and control. Elsevier.

Wang, T., Li, Q., Li, X., Zhao, S., Lu, Y., Huang, G., 2013. Use of hyperspectral imaging for label-free decoding and detection of biomarkers. Opt. Lett. 38 (9), 1524-1526.

Weeranantanaphan, J., Downey, G., Allen, P., Sun, D.W., 2011. A review of near infrared spectroscopy in muscle food analysis: 2005-2010. J. Near Infrared Spectrosc. 19 (2), 61-104.

Williams, P., 2001. Near-infrared technology in the agricultural and food industries. American Association of Cereal Chemists, St. Paul, Minnesota, USA.

Zabalza, J., Ren, J., Ren, J., Liu, Z., Marshall, S., 2014a. Structured covariance principal component analysis for real-time onsite feature extraction and dimensionality reduction in hyperspectral imaging. Appl. Opt. 53 (20), 4440-4449

353 Zabalza, J., Ren, J., Wang, Z., Marshall, S., Wang, J., 2014b. Singular spectrum analysis for
354 effective feature extraction in hyperspectral imaging. IEEE Geosci. Remote Sens. Lett. 11 (11),
355 1886-1890.

356 Zabalza, J., Ren, J., Yang, M., Zhang, Y., Wang, J., Marshall, S., Han, J., 2014c. Novel folded-
357 PCA for improved feature extraction and data reduction with hyperspectral imaging and SAR
358 in remote sensing. ISPRS J. Photogramm. Remote Sens. 93 (7), 112-122.

359 Zabalza, J., Ren, J., Zheng, J., Han, J., Zhao, H., Li, S., Marshall, S., 2015. Novel two-
360 dimensional singular spectrum analysis for effective feature extraction and data
361 classification in hyperspectral imaging. IEEE Trans. Geosci. Remote Sens. 53 (8), 4418-4433.

362 Zhao, C., Li, X., Ren, J., Marshall, S., 2013. Improved sparse representation using adaptive
363 spatial support for effective target detection in hyperspectral imagery. Int. J. Remote Sens.
364 34 (24), 8669-8684.